

Low-Temperature Route to Direct Amorphous to Rutile Crystallization of TiO₂ Thin Films Grown by Atomic Layer Deposition

Jesse Saari, Harri Ali-Löytty,* Kimmo Lahtonen, Markku Hannula, Lauri Palmolahti, Antti Tukiainen, and Mika Valden*



Cite This: *J. Phys. Chem. C* 2022, 126, 15357–15366



Read Online

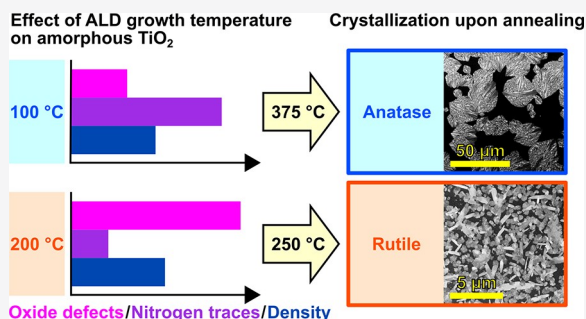
ACCESS |

Metrics & More

Article Recommendations

Supporting Information

ABSTRACT: The physicochemical properties of titanium dioxide (TiO₂) depend strongly on the crystal structure. Compared to anatase, rutile TiO₂ has a smaller bandgap, a higher dielectric constant, and a higher refractive index, which are desired properties for TiO₂ thin films in many photonic applications. Unfortunately, the fabrication of rutile thin films usually requires temperatures that are too high (>400 °C, often even 600–800 °C) for applications involving, e.g., temperature-sensitive substrate materials. Here, we demonstrate atomic layer deposition (ALD)-based fabrication of anatase and rutile TiO₂ thin films mediated by precursor traces and oxide defects, which are controlled by the ALD growth temperature when using tetrakis(dimethylamido)titanium(IV) (TDMAT) and water as precursors. Nitrogen traces within amorphous titania grown at 100 °C inhibit the crystal nucleation until 375 °C and stabilize the anatase phase. In contrast, a higher growth temperature (200 °C) leads to a low nitrogen concentration, a high degree of oxide defects, and high mass density facilitating direct amorphous to rutile crystal nucleation at an exceptionally low post deposition annealing (PDA) temperature of 250 °C. The mixed-phase (rutile–brookite) TiO₂ thin film with rutile as the primary phase forms upon the PDA at 250–500 °C that allows utilization in broad range of TiO₂ thin film applications.



INTRODUCTION

Titanium dioxide (TiO₂) is one of the most widely applied and studied photocatalyst materials, being earth-abundant, non-toxic, and stable in various environments.^{1–3} Generally, TiO₂ appears in four phases: amorphous, anatase, rutile, and brookite. The first three are the most commonly used having their own advantages, whereas brookite has remained mainly inapplicable due to the challenges in fabrication of its pure form.^{4,5} Amorphous titania (am.-TiO₂) thin films, typically grown at low temperatures, can provide exceptional optical properties and charge carrier dynamics due to the disordered structure and intrinsic Ti³⁺ defects.^{6–10} However, concerning photocatalytic applications, defect-induced gap states may increase the possibility to detrimental electron–hole recombination, and the chemical instability of am.-TiO₂ without additional electrocatalysts limits the operating conditions.^{11–16} Crystalline defect-free TiO₂, instead, is chemically stable and exhibits reduced charge carrier recombination.^{12,17,18}

When comparing the two main crystalline TiO₂ phases, anatase and rutile, the metastable anatase TiO₂ is often regarded as a better photocatalyst than the thermodynamically stable rutile.³ In fact, based on recent research, rutile is photocatalytically more active in some reactions, especially, oxidative ones, whereas anatase promotes reduction reactions.¹⁹ Another interesting approach to enhance charge carrier

separation and photocatalytic activity is a controllable fabrication of anatase–rutile phase junction structures that are reported to outperform pristine single-phase anatase and rutile, e.g., in photoelectrochemical water splitting applications.^{20,21}

Unfortunately, the major challenge with rutile thin films in many applications is the need of high processing temperatures (>400 °C, often even 600–800 °C).²² Some aqueous-phase processes enable growth of rutile nanocrystals at low temperatures (<200 °C), and atomic layer deposition of the anatase–rutile mixed phase is reported around 300 °C, but particularly, methods for obtaining pure rutile thin films at low temperatures are exceedingly limited.^{23–27} Epitaxial ALD of rutile TiO₂ thin films on substrates with the rutile-structured SnO₂, RuO₂, or IrO₂ seed layer has been demonstrated around 250 °C.²⁸ Another potential way to promote rutile formation involves dopant ion-induced oxygen vacancies or oxygen-deficient growth conditions to obtain disordered oxygen

Received: July 11, 2022

Revised: August 17, 2022

Accepted: August 18, 2022

Published: August 30, 2022



sublattice enhancing the rearrangement of ions to form easier the constrained and dense rutile phase.^{21,22,29}

One possible approach to modify the defect structure of titania is atomic layer deposition, known for its controllable, uniform, and conformal thin film growth via self-limiting surface reactions.^{12,24,30,31} Previously, we have shown that intrinsic precursor traces and oxide defects are highly sensitive to ALD growth temperature when using tetrakis-(dimethylamido)titanium(IV) and water as precursors.¹⁰ Interestingly, the growth temperature is also shown to steer the crystallization process toward anatase or rutile TiO₂ phases, but understanding of this phenomenon in more detail has remained without comprehensive investigation.^{12,18}

This work shows the role of ALD growth temperature-controlled (100–200 °C) intrinsic precursor traces and oxide defects on TiO₂ thin film crystallization upon post deposition annealing (PDA, 50 min at 200–500 °C and 500 min at 250 °C). X-ray photoelectron spectroscopy (XPS) is used to investigate the evolution of intrinsic titanium (i.e., Ti³⁺ and under- and over-coordinated Ti⁴⁺) and nitrogen (TDMAT fragments or reaction byproducts) defects within the amorphous titania upon PDA in air. Surface chemical analysis together with grazing incidence X-ray diffraction (GIXRD) measurements, X-ray reflectivity (XRR), and scanning electron microscopy (SEM) offers insights into the defect-mediated crystallization of ALD TiO₂ and fabrication of the rutile–brookite TiO₂ thin film at an exceptionally low PDA temperature of 250 °C.

■ EXPERIMENTAL SECTION

Substrates. The P-doped (resistivity 1–10 Ω·cm) n-type Si(100) wafers from SIEGERT WAFER GmbH (Germany) cleaved in 10 mm × 10 mm × 0.525 mm pieces were used as substrates in all of the experiments.

Atomic Layer Deposition. The ALD of TiO₂ was carried out using a Picosun Sunale ALD R-200 Advanced reactor and tetrakis(dimethylamido)titanium(IV) (Ti(N(CH₃)₂)₄, TDMAT, electronic grade 99.999%, Sigma-Aldrich) and Milli-Q type 1 ultrapure water as precursors. To reach the proper TDMAT precursor vapor pressure, the bubbler was heated to 76 °C, and to prevent condensation of the precursor gas, the delivery line was heated to 85 °C. The water bubbler was sustained at 18 °C by a Peltier element for stability control. Argon (99.9999%, Oy AGA Ab, Finland) was used as a carrier gas. During the deposition, the continuous Ar flow in the TDMAT and H₂O lines was 100 sccm. One ALD cycle consisted of a 1.6 s TDMAT pulse followed by a 0.1 s H₂O pulse. The excess precursor was pumped away from the reaction chamber during the 6.0 s purge period between each pulse. TiO₂ films were deposited at growth temperatures of 100 and 200 °C. The required numbers of ALD cycles for 30 nm-thick TiO₂ at growth temperatures of 100 and 200 °C were 480 and 870, respectively.

Post Deposition Annealing. The post deposition annealing for the samples was performed in atmospheric air by placing the samples into a pre-heated tube furnace for 50 min. After the heat treatment, the samples were removed from the tube furnace and let to cool down freely.

X-ray Photoelectron Spectroscopy. Majority of the X-ray photoelectron spectroscopy measurements were conducted using a NanoESCA spectromicroscope system (Omicron Nanotechnology GmbH) in ultrahigh vacuum (UHV) with a base pressure below 1 × 10⁻¹⁰ mbar. In NanoESCA, focused

monochromatized Al Kα ($h\nu = 1486.5$ eV) was used as an excitation radiation for XPS. The investigation of evolution of intrinsic Ti and N defects as a function of oxidation temperature was carried out by using a non-monochromatized DAR400 X-ray source (Al Kα) and Argus hemispherical electron spectrometer (Omicron Nanotechnology GmbH). The core level XP spectra were analyzed by the least-squares fitting of Gaussian–Lorentzian lineshapes and using a Shirley-type background. Ti 2p spectra were fitted as in our previous work¹⁰ by using the Ti 2p_{3/2} reference peak shape measured for crystalline TiO₂, i.e., the six-coordinated Ti⁴⁺ peak (Ti_{6c}⁴⁺), and the amorphous disordered structure was represented by under- and over-coordinated Ti⁴⁺ (Ti_{5/7c}⁴⁺) and Ti³⁺ peaks. The binding energy scale of the spectra was calibrated by fixing the O²⁻ peak of TiO₂ to 530.20 eV. CasaXPS version 2.3.22 PR1.0³² was used as an analysis software and the Scofield photoionization cross-sections as relative sensitivity factors.³³

Ultraviolet (UV) Light Treatment/Ar⁺ Ion Bombardment. Ti³⁺ defects were generated within am.-TiO₂ thin films via UV treatment and Ar⁺ ion bombardment. The treatments were carried out using a NanoESCA system (Omicron Nanotechnology GmbH) equipped with an Hg arc UV source (HBO 103 W/2 type lamp, 4.9 eV, 3 h) and an Ar⁺ ion gun (30 s with 5 kV acceleration voltage; P_{Ar} = 2.5 × 10⁻⁵ mbar).

Grazing Incidence X-ray Diffraction and X-ray Reflectivity. Structural properties of TiO₂ thin films were analyzed by GIXRD and XRR using two diffractometers (PANalytical Empyrean multipurpose and X'Pert³ MRD diffractometers) equipped with a Cu Kα X-ray source ($\lambda = 1.5406$ Å, $h\nu = 8.05$ keV). In GIXRD measurement, samples were scanned in the 2θ ranges of 24–34 and 20–52° at the grazing incidence angle of $\omega = 0.3^\circ$. The background was removed from each scan to allow easier comparison of the XRD patterns. In XRR measurement, samples were scanned in the coupled ω -2θ range of 0.5–4°. XRR data was modeled by the GenX program (version 3.5.5.) to extract TiO₂ film thickness, mass density, and surface roughness using a single-layer model of TiO₂ on a Si substrate.³⁴

Scanning Electron Microscopy. The surface morphology of TiO₂ thin films was studied by scanning electron microscopy (Zeiss Ultra 55, Carl Zeiss Microscopy GmbH). The SEM images were measured by using in-lens mode with a working distance of 2.3–2.4 mm, electron high tension (EHT) of 1.00 kV, and aperture size of 30.00 μm.

■ RESULTS AND DISCUSSION

The amount of intrinsic oxide defects and nitrogen traces in am.-TiO₂ depends on the ALD growth temperature when using TDMAT and H₂O as precursors.¹⁰ The ALD process at 100 °C leaves nitrogen containing TDMAT fragments or reaction byproducts within the am.-TiO₂ film, whereas the growth at 200 °C leads to a low nitrogen content but an increased amount of Ti³⁺. The amount of under- and over-coordinated Ti_{5/7c}⁴⁺ ions scales with the amount of Ti³⁺ defects. Furthermore, we have shown that am.-TiO₂ grown at 100 °C prefers crystallization into the anatase structure whereas 200 °C growth temperature induces direct crystallization into rutile at the same oxidative annealing temperature (400–500 °C).^{12,18} To understand how the intrinsic defects contribute to the crystallization upon post deposition annealing in air, 30 nm-thick ALD TiO₂ films grown at 100 and 200 °C were first investigated by X-ray photoelectron spectroscopy before and after PDA at 500 °C.

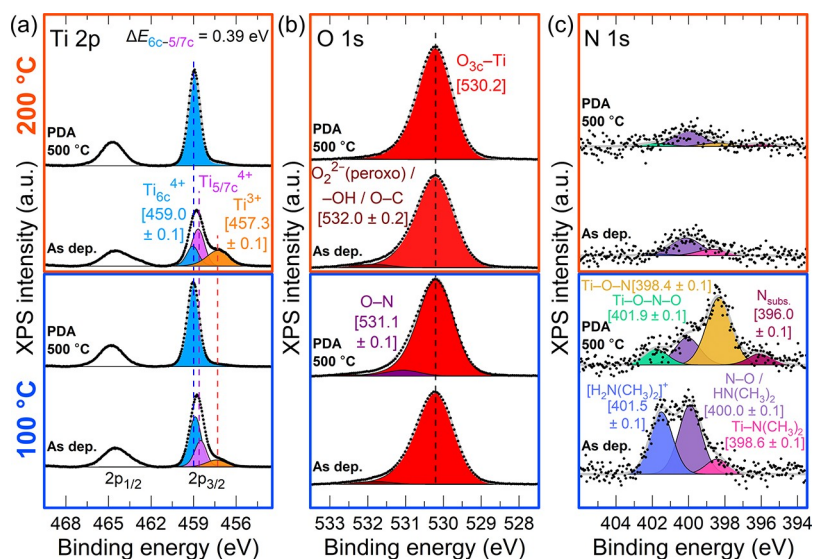


Figure 1. (a) Ti 2p, (b) O 1s, and (c) N 1s XP spectra of 30 nm-thick as-deposited and post deposition-annealed ALD TiO₂ grown at 100 and 200 °C.

Figure 1 shows Ti 2p, O 1s, and N 1s XP spectra of as-deposited amorphous and crystallized (PDA 500 °C) ALD TiO₂ grown at 100 and 200 °C (surface concentrations of elements are presented in Table S1). Figure 1a shows that oxide defects, i.e., Ti³⁺ and Ti_{5/7c}⁴⁺ defects, were completely removed from both samples upon PDA at 500 °C despite the difference in the initial amounts. Only six-coordinated Ti⁴⁺ ions (Ti_{6c}⁴⁺) were present in PDA 500 °C samples supporting the crystalline structure, i.e., Ti–O₆ octahedra are the building blocks of crystalline TiO₂.^{35,36} Few subtle changes were observed in the O 1s transition (Figure 1b) consisting of the O–Ti component (O²⁻) at 530.2 eV and minor O₂²⁻/–OH/O–C and O–N peaks at 532.0 ± 0.2 and 531.1 ± 0.1 eV, respectively. The 532.0 eV component of as-deposited samples corresponds to the interstitial peroxo (O₂²⁻) species as discussed in our previous work.¹⁰ The O 1s O–N peak was detected only in the TiO₂ (100 °C) PDA 500 °C sample. In addition, a difference was observed in the O 1s linewidths that decreased upon the PDA from 1.16 to 1.14 and 1.07 eV for 100 and 200 °C grown samples, respectively (Figure S1). The narrower O 1s linewidth is attributed to the lower nitrogen concentration and higher degree of crystalline order for the 200 °C grown sample after the PDA. It should be noted that the broader peak and a high binding energy tail of the O 1s spectra could be attributed to hydroxyl groups.^{13,37} However, the concentration of possible hydroxyl groups was too low to be reliably differentiated from the O 1s spectra, and no difference was observed between the growth temperatures.

The removal of Ti³⁺ defects upon the PDA was accompanied by the disappearance of the Ti³⁺ gap state peak at 0.3–0.4 eV from the XPS valence band spectra (Figure S2). Again, a subtle difference was observed between the growth temperatures. Upon the PDA, the valence band edge position shifted 0.20 eV toward lower binding energy for the 200 °C grown sample but no change was observed for the 100 °C grown sample. This may relate to the band gap difference between rutile TiO₂ ($E_g = 3.0$ eV) and anatase TiO₂ ($E_g = 3.2$ eV).²²

N 1s spectra in Figure 1c reveal strong difference between the samples. Nitrogen containing reaction byproducts and

TDMAT fragments within am-TiO₂ were clearly detected for the 100 °C grown sample as represented by the three components at 401.5 ± 0.1, at 400.0 ± 0.1, and at 398.6 ± 0.1 eV.^{10,31,38} After the PDA at 500 °C, an additional component at lower binding energy (396.0 ± 0.1 eV) emerged in the ALD TiO₂ grown at 100 °C. The component at 396 eV is typically reported to relate to substitutional nitrogen located at O²⁻ sites, i.e., Ti–N-like species within the TiO₂ lattice.^{39–42} Due to dimethylamine decomposition at >275 °C,⁴³ unreacted TDMAT ligands (Ti–N(CH₃)₂) and protonated dimethylamine (H₂N(CH₃)₂⁺) species are proposed to decompose during the PDA leading to the formation of TiO₂ with Ti–O–N and Ti–O–N–O species at 398.4 ± 0.1 and 401.9 ± 0.1 eV, respectively. These species contribute to the O–N component in O 1s (Figure 1b).⁴⁴ The formation mechanism of these nitrogen species within the TiO₂ lattice is discussed in more detail in Figure 4. The N 1s signal detected at 400.0 ± 0.1 eV was assigned to dimethylamine ALD process byproducts (HN(CH₃)₂) and their decomposed and oxidized N–O species locating primarily at the surface from where these species may have partially desorbed during the PDA. Indeed, in our previous study, these species (N 1s at 400.0 ± 0.1 eV) showed strong surface enrichment (1.8 at.% vs initial 0.2 at.%) after similar PDA at 350 °C that resulted in partial crystallization.¹² Therefore, it is suggested that the desorption of dimethylamine species is followed by crystallization and the remaining nitrogen species at higher temperatures are oxidized to N–O species that have similar N 1s binding energy with dimethylamine. Surface decomposition of pure dimethylamine takes place at >275 °C, and therefore, it is unlikely to have these species at the surface after PDA at 500 °C.⁴³ Compared to the am-TiO₂ thin film grown at 100 °C, only a minor amount of nitrogen was observed in ALD TiO₂ grown at 200 °C.

Despite the strong chemical changes in Ti and N species upon the PDA, only subtle changes were observed in the elemental surface concentrations (Table S1). The O²⁻/Ti ratio was close to 2 for all the samples suggesting stoichiometric TiO₂, although ionic coordination of titanium differs between as-deposited amorphous and crystallized (PDA 500 °C)

TiO₂.^{10,35,36} The nitrogen concentrations were 0.9 and 0.2 at.% for the samples grown at 100 and 200 °C, respectively. In addition, all the surfaces had 2–5 at.% of carbon. Detailed analysis of carbon species in the film was compromised due to the build-up of adventitious carbon during the sample transfer via air. TiO₂ films also contain hydrogen that cannot be directly probed with XPS, but hydrogen bonded to nitrogen species was indirectly analyzed from N 1s spectra. Indeed, Xia et al. recently studied the same TDMAT + H₂O ALD process and, by using elastic recoil detection analysis (ERDA), observed elevated hydrogen concentration in ALD TiO₂ grown at 100 °C (H/Ti = 0.5) compared to the film grown at 225 °C (H/Ti = 0.1).³⁷ The difference in the hydrogen content was found to follow the same growth temperature trend with N-bearing TDMAT fragments.

Grazing incidence X-ray diffraction measurements were conducted to study the crystallization of 30 nm-thick ALD TiO₂ grown at 100 and 200 °C upon PDA at 300, 400, and 500 °C. Figure 2a reveals that am.-TiO₂ grown at 100 °C

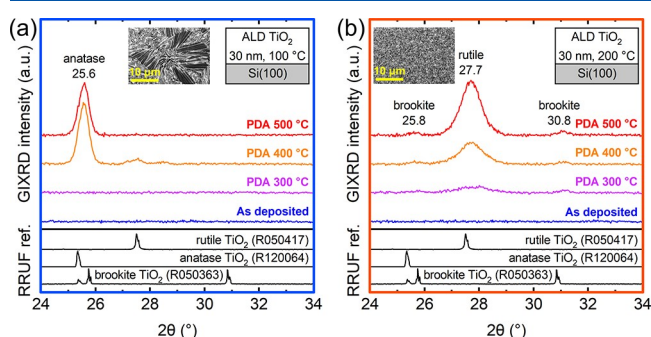


Figure 2. GIXRD patterns of 30 nm-thick ALD TiO₂ grown at (a) 100 °C and (b) 200 °C upon post deposition annealing. The XRD references are from the RRUF database.⁴⁵ The insets show the SEM images after PDA at 500 °C.

retains the amorphous phase during the PDA at 300 °C but shows similarly strong anatase peaks at 400 and at 500 °C, suggesting abrupt crystallization. Previously, we have observed that the abrupt am.-TiO₂ to anatase TiO₂ transition depends on the ALD growth temperature and takes place already at 300 °C for a growth temperature of 150 °C.¹⁸ In contrast, am.-TiO₂ grown at 200 °C shows gradual crystallization to mainly rutile TiO₂ already at 300 °C. In addition to the rutile phase, some brookite phase characterized by the peaks at 30.8 and 25.8° is also present after the PDA in TiO₂ grown at 200 °C. For both growth temperatures, complete crystallization was reached upon the PDA at 500 °C.^{12,18} Broader XRD peaks reflect in average smaller grain size for the rutile TiO₂ films compared to the anatase TiO₂, as supported by the SEM images in the insets of Figure 2.

As-deposited and PDA 500 °C samples were analyzed by XRR, and TiO₂ film thickness, mass density, and roughness were extracted via modeling (Figure S3 and Table 1). The thickness of the sample grown at 100 °C decreased by 3.3% during the PDA, while only a marginal change was observed in the 200 °C grown sample. The densities of TiO₂ films grown at 100 and 200 °C were 3.5 and 3.9 g/cm³, respectively. The PDA induced a small decrease in film roughness but had only little if any effect on the film density. The difference in film densities after the PDA can be understood by the higher bulk density of rutile vs anatase TiO₂ (4.2 vs 3.9 g/cm³). Quite

Table 1. XRR Modeling Results for 30 nm-Thick ALD TiO₂ Grown at 100 and 200 °C on Si after Deposition and after Post Deposition Annealing at 500 °C

	TiO ₂ density (g/cm ³)	TiO ₂ thickness (nm)	TiO ₂ roughness (nm)
100 °C, as-deposited	3.52	30.4	0.83
100 °C, PDA 500 °C	3.50	29.4	0.73
200 °C, as-deposited	3.94	33.5	1.06
200 °C, PDA 500 °C	3.93	33.6	0.91

surprisingly, the apparent mass densities did not change upon crystallization. The decrease in film thickness in the case of the 100 °C grown sample is likely due to the desorption of excess precursor traces and re-structuring of the film.

These density results are concordant with the values reported by Abendroth et al. for am.-TiO₂ grown by using the TDMAT + H₂O ALD process at growth temperatures of 120–200 °C.²⁷ The density increased from 3.65 g/cm³ (120 °C) to 3.95 g/cm³ (200 °C) and reached the highest value of 4.1 g/cm³ at growth temperatures of 320–330 °C, resulting in an anatase–rutile mixed phase with a relatively high N concentration of around 6 at.%. Furthermore, Busani and Devine reported similar densities for anatase (3.62 g/cm³) and mixed anatase–rutile (3.85 g/cm³) TiO₂ thin films deposited by PECVD, but before the PDA at 600 °C, the density of their am.-TiO₂ was smaller (3.2 g/cm³).⁴⁶ Piercy et al. observed ALD TiO₂ film density to increase with growth temperature from 3.3 g/cm³ (38 °C) to 3.8 g/cm³ (150 °C) when using TiCl₄ and H₂O as precursors.⁴⁷ Also, the concentration of trace Cl⁻ within the TiO₂ films decreased with the growth temperature and was reported to significantly decrease with TiO₂ crystallization above 160 °C. Go et al. fabricated ALD TiO₂ at 80 °C with TDMAT and O₃ using a process where crystallization was induced by the duration of oxygen plasma exposure during the ALD growth cycle.⁴⁸ Short (3 s) plasma exposure resulted in less dense (3.73 g/cm³) am.-TiO₂, while 30 s plasma exposure was sufficient to grow anatase TiO₂ with a density of 4.15 g/cm³. The duration of O₃ plasma exposure affected also to the amount of N traces within the TiO₂ film and was <2 at.% for the two samples.

Concerning rutile formation, Rafeian et al. reported that tuning of the oxygen concentration during reactive magnetron sputtering can be utilized to fabricate sub-stoichiometric and stoichiometric am.-TiO₂, which crystallize into rutile and anatase upon annealing in air at 500 °C, respectively.²⁹ Furthermore, according to Li et al., oxygen deficiency prefers rutile formation upon rapid thermal annealing (RTA) at 800 °C for 4 min.²¹ However, even though the am.-TiO₂ grown at 200 °C showed a considerable concentration of Ti³⁺, the film was not oxygen-deficient as the O²⁻/Ti ratio was close to 2, and still, the film crystallized as rutile.

The difference in ALD TiO₂ crystallization was mediated by the ALD growth temperature that affected essentially the concentration of oxide defects and nitrogen traces. Thus, we tested if the crystallization could be steered toward rutile by the introduction of Ti³⁺ defects, i.e., oxygen vacancies, to the as-deposited TiO₂ using UV light treatment and Ar⁺ ion bombardment (Figures S4 and S5). The test was performed using ALD TiO₂ grown at 150 °C that contains less nitrogen traces compared to TiO₂ grown at 100 °C but still favors crystallization to anatase TiO₂.^{10,18} Neither the UV light treatment nor the Ar⁺ ion bombardment changed the

crystallization from anatase upon the PDA at 500 °C, even though the concentration of Ti^{3+} defects, within XPS information depth, exceeded that of the 200 °C grown sample. Thus, the result suggests that Ti^{3+} defects were not the declarative factor determining the crystallization.

Crystallization to anatase TiO_2 is more common for PDA temperatures <500 °C. McDowell et al. reported that am- TiO_2 grown from TDMAT and H_2O at 150 °C, containing nitrogen impurities but no Ti^{3+} , crystallized into the anatase phase upon 1 h of annealing in air at 500 °C.⁴⁹ Furthermore, Pore et al. found that nitrogen and particularly Ti–N bonds prefer formation of pure anatase instead of the anatase–rutile mixed phase.⁵⁰ Similar results were also reported by Cheng et al. who considered the anatase phase stabilization to occur due to the compressive stress induced by substitutional nitrogen ions preventing the formation of more dense rutile TiO_2 .⁵¹ Regarding the anatase to rutile phase transition due to the ionic size effect, nitrogen presumably inhibits the phase transformation, but on the other hand, oxygen vacancies induced by N doping should promote rutile formation.²² Our results suggest that intrinsic nitrogen defects in am- TiO_2 delay and steer the crystallization toward anatase TiO_2 , and without nitrogen traces, a more dense am- TiO_2 favors crystallization to also more dense rutile TiO_2 .

The scanning electron microscopy images in the insets of Figure 2a,b highlight the prominent difference in the morphology and grain size of anatase and rutile TiO_2 (PDA 500 °C). The same SEM images in a larger image size are presented in Figure 3. ALD TiO_2 grown at 100 °C exhibits

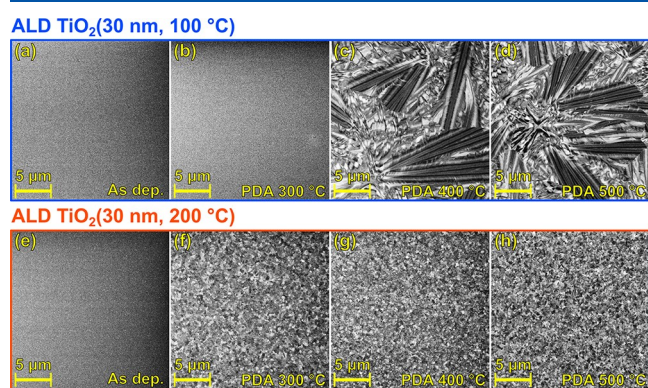


Figure 3. SEM images of 30 nm-thick ALD TiO_2 grown at (a–d) 100 °C and (e–h) 200 °C: (a, e) as-deposited and after post deposition annealing (50 min) at (b, f) 300 °C, (c, g) 400 °C, and (d, h) 500 °C. All the images were taken with the same magnification.

exceptionally large anatase grains with a lateral size of >10 μm , which is over 300 times larger than the film thickness. Based on literature, anatase grains with similar magnitude of size have been fabricated by post deposition annealing of ALD grown amorphous Ti–Nb–O or Ti–Ta–O mixed oxide films.⁵² Crystallization of undoped ALD grown am- TiO_2 into anatase is reported to result in micron-wide grains, instead.^{49,53} The rutile thin film (PDA-treated TiO_2 grown at 200 °C), by contrast, consists of much smaller grains (<1 μm).

As implied by GIXRD results (Figure 2) and sizes of the anatase and rutile grains, the crystallization kinetics of ALD am- TiO_2 grown at 100 and 200 °C are totally different. Figure 3 shows that full crystalline coverage on TiO_2 grown at 200 °C is obtained already during PDA at 300 °C (Figure 3f), whereas TiO_2 grown at 100 °C shows no crystal nucleation after the same PDA treatment (Figure 3b). However, during PDA at 400 °C (Figure 3c), large grains appear in a 100 °C grown film. To find the nucleation temperature of ALD TiO_2 grown at 100 °C, the PDA temperature range of 300–400 °C was studied in more detail. Figure S6 reveals that, upon PDA 350 °C treatment, some tiny crystal nuclei appear probably due to random impurities or defects but PDA at 375 °C leads to partial surface crystallization with large round grains with a diameter over 10 μm .

To understand how the oxide defects and nitrogen precursor traces evolve upon crystallization of ALD TiO_2 , the Ti and N species at the surface were analyzed as a function of PDA temperature. Figure 4 shows the Ti and N species (cf., Figure 1) for the N-rich ALD TiO_2 grown at 100 °C (Figure S8 shows the XPS spectra). The concentration of Ti defects (Ti^{3+} and $\text{Ti}_{5/7c}^{4+}$ species) was shown to decrease gradually with increasing PDA temperature until they disappeared completely at 400 °C that coincided with the crystallization. In the case of ALD TiO_2 grown at 200 °C, the Ti defects disappeared already at 250 °C (Figures S7 and S9) in line with the lower crystallization temperature. The evolution of N species in the case of the 200 °C grown sample was included in our previous work; besides 350 °C PDA temperature where surface enrichment of 1.8 at.% N (N 1s at 400.0 ± 0.1 eV) was detected, the amount of N at the surface was too low (0.2 at.%) for the analysis.¹² In contrast, N species in ALD TiO_2 grown at 100 °C showed a clear evolution with PDA temperature while there was only a slight decrease in the total amount of surface N (from 0.86 to 0.78 at.% N and from 2.8 to 1.8 at.% N/Ti). As the temperature increased from 200 to 400 °C, the amount of protonated dimethylamine ($\text{H}_2\text{N}(\text{CH}_3)_2^+$ reaction byproducts (i.e., $\text{HN}(\text{CH}_3)_2$ reacted with the –OH group at 401.5 eV) decreased with a rather

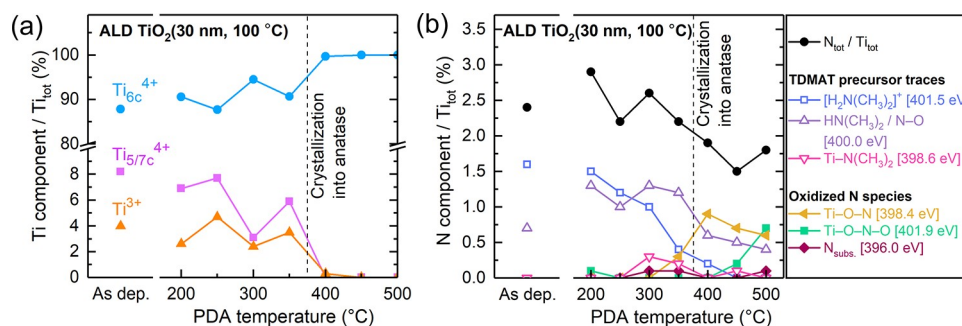
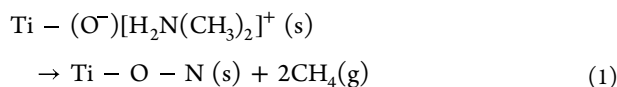


Figure 4. Evolution of (a) Ti and (b) N species as a function of the PDA temperature for 30 nm-thick ALD TiO_2 grown at 100 °C. The binding energy values of N 1s components in panel (b) are depicted in brackets.

concomitant increase in Ti–O–N species (at 398.4 eV). Thus, it is suggested that, during the PDA, N–C bonds break and CH₄ desorbs as follows



For the PDA temperature above crystallization, a high binding energy component appears in N 1s at 401.9 eV, slightly above the H₂N(CH₃)₂⁺ component observed for lower temperatures at 401.5 eV. The binding energy corresponds to strongly oxidized nitrogen species,⁵⁴ and it is suggested that, for temperatures >400 °C, Ti–O–N species oxidize to Ti–O–N–O. Substitutional nitrogen (N 1s at 396.0 eV) appeared for temperatures above the crystallization temperature (400 °C). Such substitutional N species induce visible-light absorption that is desirable in photocatalysis.³⁹ However, in our case, the amount of substitutional nitrogen was too small to induce visible-light absorption (cf., Figure S1c in ref 18). In addition, at 300 °C, a minor increase in the N 1s peak component at 400.0 eV was observed for the ALD TiO₂ grown at 100 °C, which suggests surface segregation and subsequent desorption of HN(CH₃)₂ that were observed to take place at 350 °C for the ALD TiO₂ grown at 200 °C.¹² Furthermore, these dimethylamine reaction byproducts and unreacted TDMAT ligands (at 398.6 eV) will likely react or oxidize to N–O-like species during the annealing.

Nitrogen is known to inhibit the TiO₂ crystal nucleation and raise the nucleation temperature.⁵⁵ Nitrogen also stabilizes the anatase phase.^{22,51} According to Hukari et al., the nucleation onset temperature of stoichiometric am.-TiO₂ is in the range of 250–300 °C, whereas an additional nitrogen content can raise the nucleation temperature up to 400 °C.⁵⁵ Our results show that the excess of N-bearing TDMAT fragments or reaction byproducts within am.-TiO₂ can cause the aforementioned N-mediated effects. Nitrogen defects can also contribute to the exceptionally large anatase crystal size detected for ALD TiO₂ grown at 100 °C. Similarly large crystals have been observed to result from explosive crystallization of Ti–Nb–O or Ti–Ta–O mixed oxide films prepared by Pore et al.⁵² In the explosive crystallization process, the amorphous material crystallizes rapidly in a self-sustaining manner due to the latent heat released during the crystallization and consequently inducing further amorphous material to convert into crystalline form.^{52,56,57} Although the explosive crystallization is an autocatalytic phenomenon, the speed of the process depends still on the temperature and orientation of the crystal growth.⁵⁶ However, as shown in Figure S6c and in the work by Pore et al., crystallization fronts proceed until collision with an adjacent grain and therefore inhibited nucleation and low distribution density of crystal nuclei is a desired feature when targeting formation of exceptionally large grains.^{52,58} By increasing temperature, further energy barriers for nucleation are overcome and complete crystallization is obtained (Figure S6d).⁵²

In contrast to the ALD TiO₂ grown at 100 °C, the ALD TiO₂ grown at 200 °C containing only little N traces evidences strictly different crystallization properties. As shown in Figure 5a, the ALD TiO₂ grown at 200 °C shows partial surface crystallization already at 250 °C. Furthermore, Figure 5 depicts that extending the PDA duration at 250 °C from 50 min (Figure 5a) to 500 min (Figure 5b) resulted in complete surface crystallization with crystal size <1 μm. The GIXRD

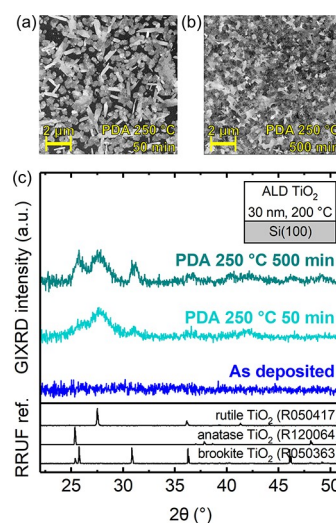


Figure 5. SEM images of 30 nm-thick ALD TiO₂ grown at 200 °C after PDA at 250 °C (a) for 50 min and (b) for 500 min. (c) GIXRD patterns of the samples. The XRD references are from the RRUF database.⁴⁵

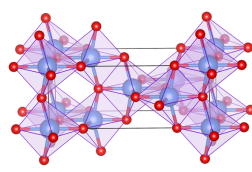
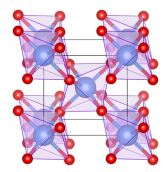
patterns (Figure 5c) show both rutile and brookite TiO₂ peaks indicating the mixed-phase TiO₂ thin film with rutile as the primary phase. The rutile to brookite ratio was found to increase with increasing PDA temperature (cf. Figure 2).

Two distinct crystal morphologies were observed after crystal nucleation of am.-TiO₂: needle- and round-like crystals (Figure 5a). Li et al. stated that the preferential growth of different rutile crystal morphologies in the aqueous-phase process is attributed to the concentration of TiOH³⁺ ions around the TiO₂ nucleus.²⁵ A low TiOH³⁺ concentration around the nucleus induces needle-like morphology, whereas a high concentration prefers radial growth of crystalline material. Comparing this crystallization mechanism to our observations, we propose that the different crystal morphologies may be analogously induced by local variations in oxide defect density within the am.-TiO₂ structure.

In general, the crystallization of am.-TiO₂ can be considered a random process that is affected by many factors. Nucleation, i.e., how TiO₆ octahedra join each other, determines whether am.-TiO₂ crystallizes as anatase or rutile.⁵⁹ Growth of metastable anatase is statistically more likely since there are more possibilities for octahedra to join at right angles compared to joining linearly sharing two edges required for the rutile phase.²² Apparently, the chemical composition and structure of the am.-TiO₂ thin film predetermined the resulting phase structure upon the PDA. We note that the crystallization can be affected by, for example, film thickness, substrate, and PDA process parameters that should be studied separately. Also, it is worth pointing out that crystallization can proceed at even lower temperatures if the duration of the PDA treatment is extended.

The effects of intrinsic defects on crystallization of ALD am.-TiO₂ upon PDA are summarized in Table 2. Lower growth temperature (100 °C) prefers trapping of TDMAT-based nitrogen species that leads to delayed crystal nucleation (at 375 °C) and exceptionally large anatase grains (>10 μm). Higher ALD growth temperature (200 °C) results in higher mass density and higher concentration of intrinsic oxide defects but less nitrogen traces. Interestingly, this am.-TiO₂ favors direct crystallization into mixed rutile-brookite phase TiO₂ with rutile

Table 2. Summary of Growth and Crystallization of am.-TiO₂ Thin Films Grown by ALD Using TDMAT and H₂O Precursors at the Growth Temperatures of 100 and 200 °C

		ALD growth temperature	
		100 °C	200 °C
As-deposited	Precursor traces ^a	+++	+
	Oxide defects ^b	+	+++
	Mass density	3.5 g/cm ³	3.9 g/cm ³
Post deposition annealing	Crystal nucleation observed at ^c	375 °C	250 °C
	Primary phase ^d	 ANATASE	 RUTILE (BROOKITE) ^e

^aNitrogen species originated from dimethylamide ligands of TDMAT molecules. The plus signs represent the surface concentration determined by the XPS measurement. ^bOxygen vacancies, interstitial peroxo species (O₂²⁻), and Ti³⁺/Ti_{5/7c}⁴⁺ ions formed via displacement of oxygen ions within the stoichiometric amorphous TiO₂ structure. The plus signs represent the surface concentration determined by the XPS measurement. ^cThe results are based on a PDA time of 50 min. ^dThe drawings of crystalline TiO₂ structures were produced by VESTA software⁶³ using rutile⁶⁴ and anatase⁶⁵ crystal structure models provided by the American Mineralogist Crystal Structure Database.⁶⁶ ^eRutile is the main phase. The proportion of brookite decreases at higher PDA temperatures.

as the primary phase already at 250 °C, which is exceptionally low for TiO₂ thin films. ALD of the anatase–rutile mixed phase thin film has been reported at 300 °C.^{23,24,27} Fabrication of rutile-rich thin films at relatively low temperature is of interest in optical and photocatalytic applications since rutile exhibits optically anisotropic nature, a high refractive index, and desirable catalytic activity in oxidation reactions.^{3,19,60} Lowering the fabrication temperature of photocatalytically active TiO₂ thin films enables applications involving temperature-sensitive materials such as polymers. Furthermore, enabling low processing temperatures (250–400 °C) to form rutile-rich TiO₂ thin films without an additional seed layer is of interest for high- κ applications, such as dynamic random-access memory (DRAM) capacitors.^{61,62} Our work demonstrated that tuning the ALD TiO₂ process parameters enabled lowering the fabrication temperature of the rutile-rich TiO₂ thin film to 250 °C. Controlling the thin film defects was essential to lowering the crystallization temperature, and we believe that the provided mechanistic understanding paves the way to further optimize the process for even higher rutile purity at even lower temperatures.

CONCLUSIONS

The role of intrinsic defects on crystallization of am.-TiO₂ thin films grown by ALD using TDMAT and H₂O precursors upon PDA treatment in air was studied as a function of ALD growth temperature (100–200 °C). The am.-TiO₂ film grown at 100 °C contained 0.9 at.% of nitrogen-bearing traces of the TDMAT precursor that inhibited crystal nucleation up to 375 °C and led to explosive crystallization of large anatase grains (>10 μ m). In contrast, the am.-TiO₂ grown at 200 °C contained less precursor traces (0.2 at.% N) and crystallized into the mixed-phase (rutile–brookite) TiO₂ thin film with rutile as the primary phase at 250 °C. The concentration of

Ti³⁺ defects increased with ALD growth temperature, and upon crystallization, these oxide defects were completely removed. Increasing the amount of Ti³⁺ defects within am.-TiO₂ either by UV treatment or Ar⁺-ion sputtering did not affect the crystallization. The mass densities of ALD TiO₂ thin films were 3.5 g/cm³ for the film grown at 100 °C and 3.9 g/cm³ for the film grown at 200 °C. The mass densities did not change during the crystallization. Therefore, it is suggested that the growth of denser am.-TiO₂ mediates direct crystallization into a more dense and stable rutile phase, while the growth of less dense am.-TiO₂ with precursor traces favors crystallization into a metastable anatase phase. Often, am.-TiO₂ thin films crystallize first into anatase and subsequently transform from an anatase to rutile phase requiring typically PDA temperatures >500 °C. By controlling the ALD growth temperature, we were able to demonstrate direct amorphous to rutile-rich TiO₂ thin film fabrication at 250–500 °C that has potential applications in the fields requiring high- κ thin films such as DRAM capacitors. Moreover, the fabrication of crystalline TiO₂ thin films at an exceptionally low temperature of 250 °C enables applications involving temperature-sensitive materials such as polymers.

ASSOCIATED CONTENT

Supporting Information

The Supporting Information is available free of charge at <https://pubs.acs.org/doi/10.1021/acs.jpcc.2c04905>.

Data and analysis from XPS, SEM, XRR, and GIXRD measurements (PDF)

AUTHOR INFORMATION

Corresponding Authors

Harri Ali-Löytty – Surface Science Group, Faculty of Engineering and Natural Sciences, Tampere University, Tampere FI-33014, Finland; orcid.org/0000-0001-8746-7268; Email: harri.ali-loytt@tuni.fi

Mika Valden – Surface Science Group, Faculty of Engineering and Natural Sciences, Tampere University, Tampere FI-33014, Finland; Email: mika.valden@tuni.fi

Authors

Jesse Saari – Surface Science Group, Faculty of Engineering and Natural Sciences, Tampere University, Tampere FI-33014, Finland; orcid.org/0000-0001-6741-0838

Kimmo Lahtonen – Faculty of Engineering and Natural Sciences, Tampere University, Tampere FI-33014, Finland; orcid.org/0000-0002-8138-7918

Markku Hannula – Surface Science Group, Faculty of Engineering and Natural Sciences, Tampere University, Tampere FI-33014, Finland; orcid.org/0000-0003-1110-7439

Lauri Palmolahti – Surface Science Group, Faculty of Engineering and Natural Sciences, Tampere University, Tampere FI-33014, Finland; orcid.org/0000-0001-9992-6628

Antti Tukiainen – Faculty of Engineering and Natural Sciences, Tampere University, Tampere FI-33014, Finland

Complete contact information is available at:
<https://pubs.acs.org/10.1021/acs.jpcc.2c04905>

Notes

The authors declare no competing financial interest.

ACKNOWLEDGMENTS

We acknowledge Cliona Shakespeare for the XPS measurement series investigating the intrinsic titanium and nitrogen defects as a function of post deposition annealing temperature and Tuomo Nyssönen for the GLXRD measurements carried out at the Department of Materials Science. This work is part of the Academy of Finland Flagship Programme, Photonics Research and Innovation (PREIN) (decision number 320165) and was supported by the Academy of Finland (decision numbers 326461 and 326406), by the Jane & Aatos Erkkö Foundation (project “Solar Fuels Synthesis”), and by Business Finland (TUTLi project “Liquid Sun”) (decision number 1464/31/2019). J.S. was supported by the Vilho, Yrjö and Kalle Väisälä Foundation of the Finnish Academy of Science and Letters and L.P. by the KAUTE Foundation and Finnish Cultural Foundation.

REFERENCES

- (1) Septina, W.; Tilley, S. D. Emerging Earth-Abundant Materials for Scalable Solar Water Splitting. *Curr. Opin. Electrochem.* **2017**, *2*, 120–127.
- (2) Pelaez, M.; Nolan, N. T.; Pillai, S. C.; Seery, M. K.; Falaras, P.; Kontos, A. G.; Dunlop, P. S. M.; Hamilton, J. W. J.; Byrne, J. A.; O’Shea, K.; et al. Review on the Visible Light Active Titanium Dioxide Photocatalysts for Environmental Applications. *Appl. Catal., B* **2012**, *125*, 331–349.
- (3) Park, H.; Park, Y.; Kim, W.; Choi, W. Surface Modification of TiO₂ Photocatalyst for Environmental Applications. *J. Photochem. Photobiol., C* **2013**, *15*, 1–20.
- (4) Di Paola, A.; Bellardita, M.; Palmisano, L. Brookite, the Least Known TiO₂ Photocatalyst. *Catalysts* **2013**, *3*, 36–73.
- (5) Dambournet, D.; Belharouak, I.; Amine, K. Tailored Preparation Methods of TiO₂ Anatase, Rutile, Brookite: Mechanism of Formation and Electrochemical Properties. *Chem. Mater.* **2010**, *22*, 1173–1179.
- (6) Hu, S.; Shaner, M. R.; Beardslee, J. A.; Lichterman, M.; Bruntschwig, B. S.; Lewis, N. S. Amorphous TiO₂ Coatings Stabilize Si, GaAs, and GaP Photoanodes for Efficient Water Oxidation. *Science* **2014**, *344*, 1005–1009.
- (7) Glezakou, V.-A.; Rousseau, R. Shedding Light on Black Titania. *Nat. Mater.* **2018**, *17*, 856–857.
- (8) Sivula, K. Defects Give New Life to an Old Material: Electronically Leaky Titania as a Photoanode Protection Layer. *ChemCatChem* **2014**, *6*, 2796–2797.
- (9) Nunez, P.; Richter, M. H.; Piercy, B. D.; Roske, C. W.; Cabán-Acevedo, M.; Losego, M. D.; Konezny, S. J.; Fermin, D. J.; Hu, S.; Bruntschwig, B. S.; Lewis, N. S. Characterization of Electronic Transport through Amorphous TiO₂ Produced by Atomic Layer Deposition. *J. Phys. Chem. C* **2019**, *123*, 20116–20129.
- (10) Saari, J.; Ali-Löytty, H.; Kauppinen, M. M.; Hannula, M.; Khan, R.; Lahtonen, K.; Palmolahti, L.; Tukiainen, A.; Grönbeck, H.; Tkachenko, N. V.; et al. Tunable Ti³⁺-Mediated Charge Carrier Dynamics of Atomic Layer Deposition-Grown Amorphous TiO₂. *J. Phys. Chem. C* **2022**, *126*, 4542–4554.
- (11) Ros, C.; Andreu, T.; Morante, J. R. Photoelectrochemical Water Splitting: A Road from Stable Metal Oxides to Protected Thin Film Solar Cells. *J. Mater. Chem. A* **2020**, *8*, 10625–10669.
- (12) Ali-Löytty, H.; Hannula, M.; Saari, J.; Palmolahti, L.; Bhuskute, B. D.; Ulkuniemi, R.; Nyssönen, T.; Lahtonen, K.; Valden, M. Diversity of TiO₂: Controlling the Molecular and Electronic Structure of Atomic-Layer-Deposited Black TiO₂. *ACS Appl. Mater. Interfaces* **2019**, *11*, 2758–2762.
- (13) Hannula, M.; Ali-Löytty, H.; Lahtonen, K.; Sarlin, E.; Saari, J.; Valden, M. Improved Stability of Atomic Layer Deposited Amorphous TiO₂ Photoelectrode Coatings by Thermally Induced Oxygen Defects. *Chem. Mater.* **2018**, *30*, 1199–1208.
- (14) Correa, G. C.; Bao, B.; Strandwitz, N. C. Chemical Stability of Titania and Alumina Thin Films Formed by Atomic Layer Deposition. *ACS Appl. Mater. Interfaces* **2015**, *7*, 14816–14821.
- (15) Kriegel, H.; Kollmann, J.; Raudsepp, R.; Klassen, T.; Schieda, M. Chemical and Photoelectrochemical Instability of Amorphous TiO₂ Layers Quantified by Spectroscopic Ellipsometry. *J. Mater. Chem. A* **2020**, *8*, 18173–18179.
- (16) Saari, J.; Ali-Löytty, H.; Honkanen, M.; Tukiainen, A.; Lahtonen, K.; Valden, M. Interface Engineering of TiO₂ Photoelectrode Coatings Grown by Atomic Layer Deposition on Silicon. *ACS Omega* **2021**, *6*, 27501–27509.
- (17) Cheng, W.-H.; Richter, M. H.; May, M. M.; Ohlmann, J.; Lackner, D.; Dimroth, F.; Hannappel, T.; Atwater, H. A.; Lewerenz, H.-J. Monolithic Photoelectrochemical Device for Direct Water Splitting with 19% Efficiency. *ACS Energy Lett.* **2018**, *3*, 1795–1800.
- (18) Khan, R.; Ali-Löytty, H.; Saari, J.; Valden, M.; Tukiainen, A.; Lahtonen, K.; Tkachenko, N. V. Optimization of Photogenerated Charge Carrier Lifetimes in ALD Grown TiO₂ for Photonic Applications. *Nanomaterials* **2020**, *10*, 1567.
- (19) Yamakata, A.; Vequizo, J. J. M. Curious Behaviors of Photogenerated Electrons and Holes at the Defects on Anatase, Rutile, and Brookite TiO₂ Powders: A Review. *J. Photochem. Photobiol., C* **2019**, *40*, 234–243.
- (20) Scanlon, D. O.; Dunnill, C. W.; Buckeridge, J.; Shevlin, S. A.; Logsdail, A. J.; Woodley, S. M.; Catlow, C. R. A.; Powell, M. J.; Palgrave, R. G.; Parkin, I. P.; et al. Band Alignment of Rutile and Anatase TiO₂. *Nat. Mater.* **2013**, *12*, 798–801.
- (21) Li, A.; Wang, Z.; Yin, H.; Wang, S.; Yan, P.; Huang, B.; Wang, X.; Li, R.; Zong, X.; Han, H.; Li, C. Understanding the Anatase–Rutile Phase Junction in Charge Separation and Transfer in a TiO₂ Electrode for Photoelectrochemical Water Splitting. *Chem. Sci.* **2016**, *7*, 6076–6082.

- (22) Hanaor, D. A. H.; Sorrell, C. C. Review of the Anatase to Rutile Phase Transformation. *J. Mater. Sci.* **2011**, *46*, 855–874.
- (23) Aarik, J.; Aidla, A.; Kiisler, A.-A.; Uustare, T.; Sammelselg, V. Effect of Crystal Structure on Optical Properties of TiO₂ Films Grown by Atomic Layer Deposition. *Thin Solid Films* **1997**, *305*, 270–273.
- (24) Reiners, M.; Xu, K.; Aslam, N.; Devi, A.; Waser, R.; Hoffmann-Eifert, S. Growth and Crystallization of TiO₂ Thin Films by Atomic Layer Deposition Using a Novel Amido Guanidinate Titanium Source and Tetrakis-Dimethylamido-Titanium. *Chem. Mater.* **2013**, *25*, 2934–2943.
- (25) Li, Y.; Liu, J.; Jia, Z. Morphological Control and Photo-degradation Behavior of Rutile TiO₂ Prepared by a Low-Temperature Process. *Mater. Lett.* **2006**, *60*, 1753–1757.
- (26) Yang, K.; Zhu, J.; Zhu, J.; Huang, S.; Zhu, X.; Ma, G. Sonochemical Synthesis and Microstructure Investigation of Rod-like Nanocrystalline Rutile Titania. *Mater. Lett.* **2003**, *57*, 4639–4642.
- (27) Abendroth, B.; Moebus, T.; Rentrop, S.; Strohmeyer, R.; Vinnichenko, M.; Weling, T.; Stöcker, H.; Meyer, D. C. Atomic Layer Deposition of TiO₂ from Tetrakis(Dimethylamino)Titanium and H₂O. *Thin Solid Films* **2013**, *545*, 176–182.
- (28) Niemelä, J.-P.; Marin, G.; Karppinen, M. Titanium Dioxide Thin Films by Atomic Layer Deposition: A Review. *Semicond. Sci. Technol.* **2017**, *32*, No. 093005.
- (29) Rafeian, D.; Ogieglo, W.; Savenije, T.; Lammertink, R. G. H. Controlled Formation of Anatase and Rutile TiO₂ Thin Films by Reactive Magnetron Sputtering. *AIP Adv.* **2015**, *5*, No. 097168.
- (30) Dendooven, J.; Detavernier, C. *Atomic Layer Deposition in Energy Conversion Applications*; Bachmann, J., Ed.; John Wiley & Sons, Ltd., 2017; pp. 1–40.
- (31) Head, A. R.; Chaudhary, S.; Olivieri, G.; Bournel, F.; Andersen, J. N.; Rochet, F.; Gallet, J.-J.; Schnadt, J. Near Ambient Pressure X-ray Photoelectron Spectroscopy Study of the Atomic Layer Deposition of TiO₂ on RuO₂(110). *J. Phys. Chem. C* **2016**, *120*, 243–251.
- (32) Fairley, N.; Fernandez, V.; Richard-Plouet, M.; Guillot-Deudon, C.; Walton, J.; Smith, E.; Flahaut, D.; Greiner, M.; Biesinger, M.; Tougaard, S.; et al. Systematic and Collaborative Approach to Problem Solving Using X-ray Photoelectron Spectroscopy. *Appl. Surf. Sci. Adv.* **2021**, *5*, No. 100112.
- (33) Scofield, J. H. Hartree-Slater Subshell Photoionization Cross-Sections at 1254 and 1487 eV. *J. Electron Spectrosc. Relat. Phenom.* **1976**, *8*, 129–137.
- (34) Björck, M.; Andersson, G. GenX: An Extensible X-ray Reflectivity Refinement Program Utilizing Differential Evolution. *J. Appl. Crystallogr.* **2007**, *40*, 1174–1178.
- (35) Prasai, B.; Cai, B.; Underwood, M. K.; Lewis, J. P.; Drabold, D. A. Properties of Amorphous and Crystalline Titanium Dioxide from First Principles. *J. Mater. Sci.* **2012**, *47*, 7515–7521.
- (36) Deskins, N. A.; Du, J.; Rao, P. The Structural and Electronic Properties of Reduced Amorphous Titania. *Phys. Chem. Chem. Phys.* **2017**, *19*, 18671–18684.
- (37) Xia, B.; Ganem, J.-J.; Vickridge, I.; Briand, E.; Steydl, S.; Benbalagh, R.; Rochet, F. Water-Rich Conditions during Titania Atomic Layer Deposition in the 100 °C–300 °C Temperature Window Produce Films with Ti^{IV} Oxidation State but Large H and O Content Variations. *Appl. Surf. Sci.* **2022**, *601*, No. 154233.
- (38) Sperling, B. A.; Kimes, W. A.; Maslar, J. E. Reflection Absorption Infrared Spectroscopy during Atomic Layer Deposition of HfO₂ Films from Tetrakis(Ethylmethylamido)Hafnium and Water. *Appl. Surf. Sci.* **2010**, *256*, 5035–5041.
- (39) Asahi, R.; Morikawa, T.; Ohwaki, T.; Aoki, K.; Taga, Y. Visible-Light Photocatalysis in Nitrogen-Doped Titanium Oxides. *Science* **2001**, *293*, 269–271.
- (40) Hashimoto, K.; Irie, H.; Fujishima, A. TiO₂ Photocatalysis: A Historical Overview and Future Prospects. *Jpn. J. Appl. Phys.* **2005**, *44*, 8269.
- (41) Deng, S.; Verbruggen, S. W.; Lenaerts, S.; Martens, J. A.; Van den Bergh, S.; Devloo-Casier, K.; Devulder, W.; Dendooven, J.; Deduytsche, D.; Detavernier, C. Controllable Nitrogen Doping in as Deposited TiO₂ Film and Its Effect on Post Deposition Annealing. *J. Vac. Sci. Technol., A* **2014**, *32*, No. 01A123.
- (42) Martínez-Ferrero, E.; Sakatani, Y.; Boissière, C.; Grosso, D.; Fuentès, A.; Fraxedas, J.; Sanchez, C. Nanostructured Titanium Oxynitride Porous Thin Films as Efficient Visible-Active Photocatalysts. *Adv. Funct. Mater.* **2007**, *17*, 3348–3354.
- (43) Driessen, J. P. A. M.; Schoonman, J.; Jensen, K. F. Infrared Spectroscopic Study of Decomposition of Ti(N(CH₃)₂)₄. *J. Electrochem. Soc.* **2001**, *148*, G178.
- (44) Hsu, J.-C.; Lin, Y.-H.; Wang, P. W. X-ray Photoelectron Spectroscopy Analysis of Nitrogen-Doped TiO₂ Films Prepared by Reactive-Ion-Beam Sputtering with Various NH₃/O₂ Gas Mixture Ratios. *Coatings* **2020**, *10*, 47.
- (45) Lafuente, B.; Downs, R. T.; Yang, H.; Stone, N. The Power of Databases: The RRUFF Project. In *Highlights in Mineralogical Crystallography*; Armbruster, T.; Danisi, R. M., Eds.; Walter de Gruyter GmbH & Co KG, 2015; pp. 1–30 DOI: 10.1515/9783110417104-003.
- (46) Busani, T.; Devine, R. A. B. Dielectric and Infrared Properties of TiO₂ Films Containing Anatase and Rutile. *Semicond. Sci. Technol.* **2005**, *20*, 870–875.
- (47) Piercy, B. D.; Leng, C. Z.; Losego, M. D. Variation in the Density, Optical Polarizabilities, and Crystallinity of TiO₂ Thin Films Deposited via Atomic Layer Deposition from 38 to 150 °C Using the Titanium Tetrachloride-Water Reaction. *J. Vac. Sci. Technol., A* **2017**, *35*, No. 03E107.
- (48) Go, D.; Lee, J.; Shin, J. W.; Lee, S.; Kang, W.; Han, J. H.; An, J. Phase-Gradient Atomic Layer Deposition of TiO₂ Thin Films by Plasma-Induced Local Crystallization. *Ceram. Int.* **2021**, *47*, 28770–28777.
- (49) McDowell, M. T.; Lichterman, M. F.; Carim, A. I.; Liu, R.; Hu, S.; Brunshwig, B. S.; Lewis, N. S. The Influence of Structure and Processing on the Behavior of TiO₂ Protective Layers for Stabilization of n-Si/TiO₂/Ni Photoanodes for Water Oxidation. *ACS Appl. Mater. Interfaces* **2015**, *7*, 15189–15199.
- (50) Pore, V.; Heikkilä, M.; Ritala, M.; Leskelä, M.; Areva, S. Atomic Layer Deposition of TiO_{2-x}N_x Thin Films for Photocatalytic Applications. *J. Photochem. Photobiol., A* **2006**, *177*, 68–75.
- (51) Cheng, H.-E.; Chen, Y.-R.; Wu, W.-T.; Hsu, C.-M. Effect of Nitrogen Doping Concentration on the Properties of TiO₂ Films Grown by Atomic Layer Deposition. *Mater. Sci. Eng., B* **2011**, *176*, 596–599.
- (52) Pore, V.; Ritala, M.; Leskelä, M.; Saukkonen, T.; Järn, M. Explosive Crystallization in Atomic Layer Deposited Mixed Titanium Oxides. *Cryst. Growth Des.* **2009**, *9*, 2974–2978.
- (53) Dufond, M. E.; Chazalviel, J.-N.; Santinacci, L. Electrochemical Stability of n-Si Photoanodes Protected by TiO₂ Thin Layers Grown by Atomic Layer Deposition. *J. Electrochem. Soc.* **2021**, *168*, No. 031509.
- (54) Viswanathan, B.; Krishnamurthy, K. R. Nitrogen Incorporation in TiO₂: Does It Make a Visible Light Photo-Active Material? *Int. J. Photoenergy* **2012**, *2012*, 1–10.
- (55) Hukari, K.; Dannenberg, R.; Stach, E. A. Nitrogen Effects on Crystallization Kinetics of Amorphous TiO_xN_y Thin Films. *J. Mater. Res.* **2002**, *17*, 550–555.
- (56) Albenze, E. J.; Thompson, M. O.; Clancy, P. Molecular Dynamics Study of Explosive Crystallization of SiGe and Boron-Doped SiGe Alloys. *Ind. Eng. Chem. Res.* **2006**, *45*, 5628–5639.
- (57) Buchner, C.; Schneider, W. Explosive Crystallization in Thin Amorphous Layers on Heat Conducting Substrates. *J. Appl. Phys.* **2015**, *117*, 245301.
- (58) Cho, C. J.; Kang, J.-Y.; Lee, W. C.; Baek, S.-H.; Kim, J.-S.; Hwang, C. S.; Kim, S. K. Interface Engineering for Extremely Large Grains in Explosively Crystallized TiO₂ Films Grown by Low-Temperature Atomic Layer Deposition. *Chem. Mater.* **2017**, *29*, 2046–2054.
- (59) Petkov, V.; Holzhu, G. Atomic-Scale Structure of Amorphous TiO₂ by Electron, X-ray Diffraction and Reverse Monte Carlo Simulations. *J. Non-Cryst. Solids* **1998**, *231*, 17–30.

(60) Jellison, G. E., Jr.; Boatner, L. A.; Budai, J. D.; Jeong, B.-S.; Norton, D. P. Spectroscopic Ellipsometry of Thin Film and Bulk Anatase (TiO₂). *J. Appl. Phys.* **2003**, *93*, 9537–9541.

(61) Lee, D.-K.; Kwon, S.-H.; Ahn, J.-H. Growth of Rutile-TiO₂ Thin Films via Sn Doping and Insertion of Ultra-Thin SnO₂ Interlayer by Atomic Layer Deposition. *Mater. Lett.* **2019**, *246*, 1–4.

(62) Kim, B.; Choi, Y.; Lee, D.; Cheon, S.; Byun, Y.; Jeon, H. Atomic Layer Deposition for Rutile Structure TiO₂ Thin Films Using a SnO₂ Seed Layer and Low Temperature Heat Treatment. *Nanotechnology* **2021**, *33*, 115701.

(63) Momma, K.; Izumi, F. VESTA 3 for Three-Dimensional Visualization of Crystal, Volumetric and Morphology Data. *J. Appl. Crystallogr.* **2011**, *44*, 1272–1276.

(64) Baur, W. H. Über die Verfeinerung der Kristallstrukturbestimmung einiger Vertreter des Rutiltyps: TiO₂, SnO₂, GeO₂ und MgF₂. *Acta Cryst.* **1956**, *9*, 515–520.

(65) Howard, C. J.; Sabine, T. M.; Dickson, F. Structural and Thermal Parameters for Rutile and Anatase. *Acta Cryst. B* **1991**, *47*, 462–468.

(66) Downs, R. T.; Hall-Wallace, M. The *American Mineralogist* Crystal Structure Database. *Am. Mineral.* **2003**, *88*, 247–250.

Recommended by ACS

Hierarchical Iridium Nanostructure-Based Thin Films with High-Temperature Stability and Oxidation Resistance for Thermocouples

Bingwei Luo, Jinhua Xie, *et al.*

MARCH 04, 2022

ACS APPLIED NANO MATERIALS

READ 

Spray Pyrolysis of ZnO:In: Characterization of Growth Mechanism and Interface Analysis on p-Type GaAs and n-Type Si Semiconductor Materials

Ulrike Heitmann, Jan Neethling, *et al.*

AUGUST 30, 2022

ACS APPLIED MATERIALS & INTERFACES

READ 

Aerosol-Prepared Microcrystals as Amplifiers to Learn about the Facet and Point Defect-Dependent Lability and Stabilization of Hybrid Perovskite Semiconductors agains...

Ulrich Johannes Bahnmüller, Sebastian Polarz, *et al.*

JULY 11, 2022

CRYSTAL GROWTH & DESIGN

READ 

Direct Synthesis of Metastable λ -Phase Ti₃O₅ Films on LaAlO₃ (110) Substrates at High Temperatures

Kohei Yoshimatsu and Hiroshi Kumigashira

DECEMBER 15, 2021

CRYSTAL GROWTH & DESIGN

READ 

Get More Suggestions >